

04,05

## Synthesis, structural and magnetic properties $\text{NaZnFe}_2(\text{VO}_4)_3$

© T.V. Drokina<sup>1</sup>, M.S. Molokeev<sup>1,2</sup>, D.A. Velikanov<sup>1</sup>, O.A. Bayukov<sup>1</sup>,  
A.M. Vorotynov<sup>1</sup>, A.L. Friedman<sup>1</sup>, G.A. Petrakovsky<sup>1</sup>

<sup>1</sup> L.V. Kirensky Institute of Physics,  
Federal Research Center KSC Siberian Branch of Russian Academy of Science,  
Krasnoyarsk, Russia

<sup>2</sup> Siberian Federal University,  
Krasnoyarsk, Russia

✉ E-mail: tvd@iph.krasn.ru

Received June 30, 2023

Revised June 30, 2023

Accepted July 4, 2023

A new magnetic compound  $\text{NaZnFe}_2(\text{VO}_4)_3$  obtained by solid-phase synthesis has been studied using X-ray diffraction, Mössbauer spectroscopy, electron paramagnetic resonance, measurement of the temperature dependence of the dielectric permeability, and magnetometry.

The crystalline structure of  $\text{NaZnFe}_2(\text{VO}_4)_3$  is described by a triclinic spatial group of symmetry  $P1$  with the parameters of an elementary crystalline chain:  $a = 6.74318(7) \text{ \AA}$ ,  $b = 8.1729(1) \text{ \AA}$ ,  $c = 9.8421(1) \text{ \AA}$ ,  $\alpha = 106.2611(9)^\circ$ ,  $\beta = 104.55(1)^\circ$ ,  $\gamma = 102.337(1)^\circ$ ,  $V = 479.88(1) \text{ \AA}^3$ ,  $Z = 2$ . Magnetic  $\text{Fe}^{3+}$  cations in the cell occupy six positions populated together with diamagnetic  $\text{Zn}^{2+}$  cations, which leads to states of magnetic inhomogeneity and local violation of charge neutrality.

Data from resonance and magnetic studies of  $\text{NaZnFe}_2(\text{VO}_4)_3$  confirm the main role of high-spin  $\text{Fe}^{3+}$  iron cations in the formation of magnetism with competing exchange magnetic interactions and a high value of the frustration index. It is shown that the magnetic subsystem of a sample with a negative asymptotic Neel temperature undergoes a magnetic transition from the paramagnetic state to the magnetic state of the spin glass when the temperature decreases.

**Keywords:** inorganic compounds, multicomponent vanadates, crystal structure, magnetic properties.

DOI: 10.61011/PSS.2023.08.56572.134

### 1. Introduction

The search, synthesis and study of the properties of new multicomponent magnetic compounds is of interest for fundamental physics and possible applications, as well as the development of materials with a controlled degree of atomic disorder and the magnetic state of spin glass, contributing to the development of understanding the nature of their magnetism. The dependence of magnetic properties observed in the spin-glass magnetic state on the thermal prehistory of the sample may contribute to the development of magnetic information technologies.

Spin glasses have an important place among the studies of different types of magnetically ordered substances [1–3]. Examples of compounds with the magnetic state of spin glass can be disordered systems with randomly varying exchange interactions that determine the mutual orientation of the magnetic moments of atoms.

The family of compounds  $\text{RFeTi}_2\text{O}_7$  ( $\text{R} = \text{Sm} - \text{Lu}$ ) crystallizes at room temperature in the centrosymmetric orthorhombic space group  $Pcnb$  [4]. The crystal structure contains 8 formula units in an elementary cell and is constructed of four-, five-, six- and eight-vertex oxygen polyhedra. A rare-earth cation is located in the octahedron. The three nonequivalent octahedral positions in the structure

are mainly populated by titanium. Tetrahedral positions are occupied by iron. Tetrahedral cations can exit tetrahedra and populate adjacent positions with a coordination equal to five. Thus, in these compounds there is a geometric disorder in the arrangement of iron ions  $\text{Fe}^{3+}$ , which leads to frustration of magnetic interactions and a spin-glass magnetic state with characteristic static properties: the absence of anomalies on the temperature dependences of the specific heat at freezing temperature  $T_F$ , linear dependence the magnetic contribution to the heat capacity from the temperature at  $T \ll T_F$ , the dependence of magnetization on the magnetic background of the sample (cooling in a magnetic field and turning on the field after cooling to temperatures  $T < T_F$  lead to different values of the magnetic moment), as well as dynamic properties: dependence of the real part of the susceptibility  $\chi'$  on frequency, the presence of „casp“ on the temperature dependence curve  $\chi'$  [4].

Spin-glass properties are manifested by the compound  $\text{CrNbO}_4$  with the structure of rutile  $\text{TiO}_2$ , crystallizing in the tetragonal space group  $P42/mnm$  [5]. The ionic radii of metals  $\text{Cr}^{3+}$ ,  $\text{Nb}^{5+}$  located in an octahedral oxygen environment are approximately the same, so the ions are randomly distributed over octahedral positions in the crystal structure. The compound  $\text{CrNbO}_4$  passes into the spin glass state at temperatures 9.3 K [5].

$\text{Ba}_2\text{Fe}_2\text{GeO}_7$  — a representative of the family of compounds with the melilite structure  $\text{Ga}_2\text{Al}_2\text{SiO}_7$  crystallizes in the space group P421m [6]. The structure contains layers of polyhedra containing barium ions alternating along the tetragonal axis and oxygen tetrahedra of two types (T1 and T2) linked in five-membered rings. Tetrahedra T1 are populated with ions  $\text{Fe}^{3+}$ , tetrahedra T2 are populated statistically with ions  $\text{Fe}^{3+}$  and  $\text{Ge}^{4+}$  in the ratio 1:1. Neutron scattering spectra do not detect long-range magnetic order up to 2 K. There are no anomalies on the dependence of the specific heat capacity on temperature. Magnetic studies showed that antiferromagnetic interaction is the predominant interaction between magnetic cations. The dependence of magnetization on the thermal background of the sample is observed below 8 K. Experimental facts indicate the transition of the magnetic subsystem of the sample to the spin-glass state [6].

Thus, a common property of magnets with the magnetic state of spin glass is the disordered arrangement of magnetic ions in space, leading to competition and frustration of magnetic interactions.

Introduction to the structure of metal oxide vanadates with the general formula  $\text{ABFe}_2(\text{VO}_4)_3$ , where A — monovalent alkaline earth elements, B — divalent elements, various cations, affects the nature of the crystal structure, and, as a consequence, on the magnetic properties of materials with magnetic systems of reduced dimension [7–9]. We describe in this paper the conditions of synthesis and study of the structural and magnetic properties of a new magnetic material — oxide  $\text{NaZnFe}_2(\text{VO}_4)_3$ , whose crystal structure contains six non-equivalent crystallographic positions filled with magnetic iron cations  $\text{Fe}^{3+}$  and diamagnetic zinc cations  $\text{Zn}^{2+}$ . The presence of diamagnetic cations in chains of magnetic cations complicates the structure of low-dimensional magnetic elements in a 3D crystal.

## 2. Sample synthesis and experimental technique

Samples of  $\text{NaZnFe}_2(\text{VO}_4)_3$  composition were obtained by reaction in the solid phase with annealing at temperatures of 640 and 650°C for 24 h in air from a stoichiometric mixture of oxides of high purity  $\text{Na}_2\text{CO}_3$ ,  $\text{Fe}_2\text{O}_3$ ,  $\text{ZnO}$ ,  $\text{V}_2\text{O}_5$ . The chemical and phase composition of the synthesized samples was controlled by X-ray diffraction analysis.

The powder radiograph of  $\text{NaZnFe}_2(\text{VO}_4)_3$  was captured at room temperature on a Bruker D8 ADVANCE diffractometer using a VANTEC linear detector and  $\text{Cu-K}\alpha$  radiation. Different sizes of primary beam slits were used during the experiment: 0.6 mm in the range of angles  $2\theta = 5^\circ - 70^\circ$  and 2 mm in the range of  $70^\circ - 120^\circ$ . The scanning interval is  $0.016^\circ$  and remained constant in all sections. The exposure time at each interval is 2.7 s and 1.8 s for the ranges  $5^\circ - 70^\circ$  and  $70^\circ - 120^\circ$ , respectively. Subsequently, the standard deviations of the intensities of all

points of the X-ray were calculated, and then the intensities and standard deviations of all points of the high-angle part were multiplied by a normalizing coefficient of 0.45.

The magnetic properties of the  $\text{NaZnFe}_2(\text{VO}_4)_3$  magnet were studied using SQUID magnetometer designed by the Kirensky Institute of Physics of Federal Research Center KSC of Siberian Branch of RAS [10]. Static magnetic characteristics were measured in the temperature range 4–300 K in two modes: cooling of the sample without a magnetic field (ZFC) and in a magnetic field (FC).

The behavior of the dielectric constant in the temperature range  $2.3 \text{ K} < T < 33 \text{ K}$  at the frequency  $f = 100 \text{ kHz}$  is studied. A conductive epoxy adhesive with a silver filler was applied to the opposite planes of the sample made in the form of a disk with a diameter of  $\sim 12 \text{ mm}$ , and a thickness of  $\sim 1.5 \text{ mm}$ . The electrical capacitance of the resulting capacitor was measured using Agilent E4980A meter. The dielectric constant is calculated in the approximation of the model of a flat capacitor.

The electron magnetic resonance spectra were taken on a Bruker Elexsys E580 spectrometer in the X-band ( $\nu = 9 \text{ GHz}$ ) and the temperature range 110–300 K. The following parameters were used for spectrum recording: microwave power — 0.63 mW, modulation amplitude — 0.7 G, modulation frequency — 100 kHz, magnetic field sweep width — 5 kG, sweep time — 40 s.

Nuclear gamma resonance spectra were recorded using MS-1104Em spectrometer of the Kirensky Institute of Physics of the Siberian Branch of RAS at room temperature with a source of  $\text{Co}^{57}(\text{Rh})$  on powders with a thickness of  $5 - 10 \text{ mg/cm}^2$  based on the natural iron content. The values of chemical shifts are given relative to  $\alpha\text{-Fe}$ .

## 3. Experimental results and discussion

### 3.1. Structural properties of $\text{NaZnFe}_2(\text{VO}_4)_3$

The solution of the crystal structure of  $\text{NaZnFe}_2(\text{VO}_4)_3$  was performed on the basis of X-ray diffraction analysis data. Figure 1 shows a powder radiograph of the compound obtained at room temperature.

Almost all reflexes (except low intensity peaks belonging to the impurity  $\text{ZnFe}_2\text{O}_4$  ( $\sim 2\%$  by weight)) were indicated by a triclinic cell with parameters close to those of  $\text{NaFe}_3(\text{VO}_4)_3$  [11], so its structure was used as the source. Since the occupation density of Fe/Zn was extremely unstable due to the proximity of atomic scattering functions, all six positions of Fe ions were occupied with Fe/Zn ions with fixed occupation densities of positions according to the chemical formula  $\text{Fe/Zn} = 2:1$ . The coordinates of Na1 were not refined, which is required to fix the origin in the polar group P1. The Rietveld refinement is implemented using the TOPAS 4.2 [12] program. The results of the refinement are shown in Table 1 and Fig. 1. The atomic coordinates and thermal parameters are presented in Table 2, the main bond lengths are shown in Table 3.

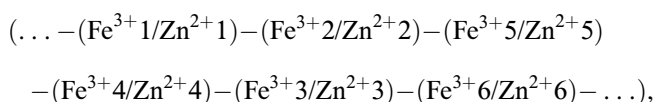
**Table 1.** The main parameters of the X-ray experiment conducted at a temperature of  $T = 300$  K, and the results of the refinement of the crystal structure of  $\text{NaZnFe}_2(\text{VO}_4)_3$ 

| Pr. gr.               | $P1$         |
|-----------------------|--------------|
| $a$ , Å               | 6.74318 (7)  |
| $b$ , Å               | 8.1729 (1)   |
| $c$ , Å               | 9.8421 (1)   |
| $\alpha$ , °          | 106.2611 (9) |
| $\beta$ , °           | 104.55 (1)   |
| $\gamma$ , °          | 102.337 (1)  |
| $V$ , Å <sup>3</sup>  | 479.88 (1)   |
| $2\theta$ interval, ° | 5–120        |
| $R_{\text{wp}}$ , %   | 1.10         |
| $R_{\text{p}}$ , %    | 1.00         |
| $R_{\text{B}}$ , %    | 0.40         |
| $\chi^2$              | 1.46         |

Note.  $a$ ,  $b$ ,  $c$ ,  $\alpha$ ,  $\beta$ ,  $\gamma$  — lattice cell parameters;  $V$  — cell volume; unreliability factors:  $R_{\text{wp}}$  — weight profile,  $R_{\text{p}}$  — profile,  $R_{\text{B}}$  — integral;  $\chi^2$  — fit quality.

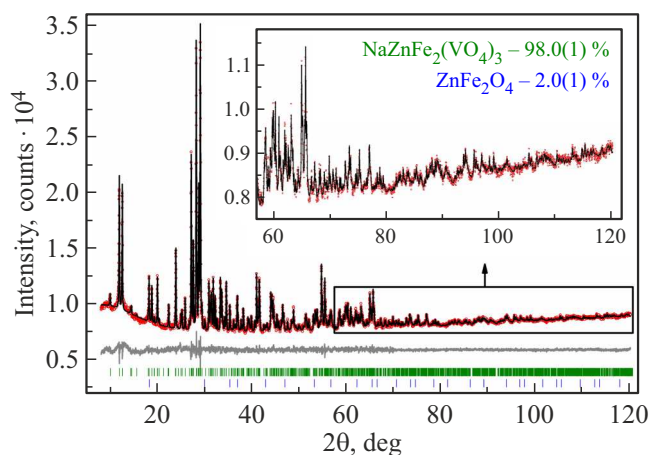
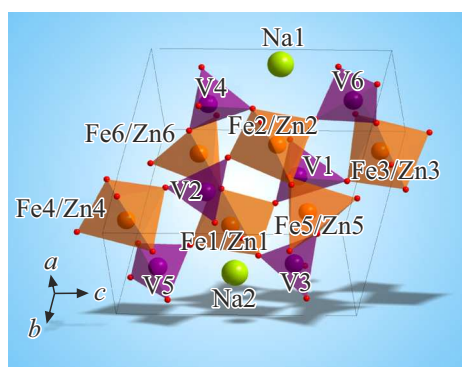
According to X-ray diffraction data, the crystal structure of multicomponent vanadate  $\text{NaZnFe}_2(\text{VO}_4)_3$  is described by a triclinic space symmetry group  $P1$ . The lattice cell of the studied compound contains two formula units ( $Z = 2$ ). The charge composition of the compound has the form  $\text{Na}^+\text{Zn}^{2+}\text{Fe}_2^{3+}(\text{V}^5+\text{O}_4^{2-})_3$ .

The crystal structure of  $\text{NaZnFe}_2(\text{VO}_4)_3$  is shown in Fig. 2. There are six nonequivalent crystallographic positions  $\text{Fe}_i/\text{Zn}_i$  ( $i = 1-6$ ) in the structure, four of them with an octahedral oxygen environment, and two with an environment in the form of a trigonal bipyramid. Compounds  $(\text{Fe}_i^{3+}/\text{Zn}_i^{2+})\text{O}_j$  ( $j = 5, 6$ ) are interconnected by common vertices and form infinite chains



stretching along the direction  $a-c$ . The chains are linked to each other by tetrahedral anionic complexes  $(\text{VO}_4)^{3-}$ , forming a two-dimensional layer that is in a plane based on two vectors  $a-c$  and  $b$ . The layers are linked by bundles  $\text{VO}_4$ , forming a three-dimensional structure. The channels of the structure are filled with cations  $\text{Na}^+$ , which occupy two nonequivalent crystallographic positions.

In the lattice crystal cell  $\text{NaZnFe}_2(\text{VO}_4)_3$  iron cations  $\text{Fe}^{3+}$  are occupied together with cations  $\text{Zn}^{2+}$  (Table 2), then there is a localization of cations of different grades and valence in the same crystal position. Depending on the ratio of iron and zinc ions, an excess or lack of

**Figure 1.** Difference radiograph of polycrystalline compound  $\text{NaZnFe}_2(\text{VO}_4)_3$  at  $T = 300$  K.**Figure 2.** Crystal structure of the compound  $\text{NaZnFe}_2(\text{VO}_4)_3$  at room temperature.

positive charge is formed in one crystallographic position, which leads to the realization of a state of local violation of charge neutrality.

A Mössbauer study was conducted to assess the state of iron in the sample  $\text{NaZnFe}_2(\text{VO}_4)_3$ . Figure 3, *a* shows the Mössbauer spectrum at room temperature, which is a quadrupole doublet. The probability distribution of quadrupole cleavages in the experimental spectrum was determined to clarify the question of the presence of nonequivalent iron positions in the sample, Fig. 3, *b*. Peaks on the P(QS) distribution indicate possible non-equivalent positions.

The model spectrum formed on the basis of information obtained from the P(QS) dependence and consisting of two doublets is adjusted to the experimental spectrum when all parameters of the hyperfine structure are varied. The results of the spectrum interpretation are summarized in Table 4.

The values of chemical shifts correspond to iron cations in the trivalent ( $\text{Fe}^{3+}$ ) and high-spin ( $S = 5/2$ ) state.

The spectrum is dominated by a signal from iron cations with an octahedral oxygen environment characterized by an isomeric chemical shift relative to  $\alpha\text{-Fe IS} = 0.39$  mm/s,

**Table 2.** Atomic coordinates, isotropic thermal parameters  $B_{\text{iso}}$  ( $\text{\AA}^2$ ) and population of positions (Occ.) in the crystal structure of  $\text{NaZnFe}_2(\text{VO}_4)_3$  at temperature  $T = 300 \text{ K}$ 

| Atom | $x/a$      | $y/b$      | $z/c$      | $B_{\text{iso}}$ | Occ. |
|------|------------|------------|------------|------------------|------|
| Na1  | 0.99425    | 0.07762    | 0.5534     | 3.0 (8)          | 1    |
| Na2  | 0.555 (6)  | 1.016 (5)  | 0.529 (4)  | 0.5 (6)          | 1    |
| Fe1  | 0.132 (6)  | 0.575 (4)  | 0.396 (4)  | 0.5 (2)          | 2/3  |
| Zn1  | 0.132 (6)  | 0.575 (4)  | 0.396 (4)  | 0.5 (2)          | 1/3  |
| Fe2  | 0.890 (6)  | 0.467 (4)  | 0.613 (4)  | 0.5 (2)          | 2/3  |
| Zn2  | 0.890 (6)  | 0.467 (4)  | 0.613 (4)  | 0.5 (2)          | 1/3  |
| Fe3  | 0.457 (6)  | 0.308 (4)  | 0.984 (4)  | 0.5 (2)          | 2/3  |
| Zn3  | 0.457 (6)  | 0.308 (4)  | 0.984 (4)  | 0.5 (2)          | 1/3  |
| Fe4  | 0.539 (6)  | 0.729 (4)  | 0.018 (4)  | 0.5 (2)          | 2/3  |
| Zn4  | 0.539 (6)  | 0.729 (4)  | 0.018 (4)  | 0.5 (2)          | 1/3  |
| Fe5  | 0.793 (6)  | 0.788 (3)  | 0.799 (4)  | 0.5 (2)          | 2/3  |
| Zn5  | 0.793 (6)  | 0.788 (3)  | 0.799 (4)  | 0.5 (2)          | 1/3  |
| Fe6  | 0.235 (6)  | 0.233 (4)  | 0.201 (4)  | 0.5 (2)          | 2/3  |
| Zn6  | 0.235 (6)  | 0.233 (4)  | 0.201 (4)  | 0.5 (2)          | 1/3  |
| V1   | 0.400 (6)  | 0.422 (4)  | 0.661 (4)  | 0.2 (2)          | 1    |
| V2   | 0.610 (6)  | 0.603 (4)  | 0.327 (4)  | 0.2 (2)          | 1    |
| V3   | 0.281 (6)  | 0.844 (3)  | 0.726 (3)  | 0.2 (2)          | 1    |
| V4   | 0.732 (6)  | 0.180 (4)  | 0.257 (4)  | 0.2 (2)          | 1    |
| V5   | 0.098 (6)  | 0.786 (4)  | 0.136 (4)  | 0.2 (2)          | 1    |
| V6   | 0.914 (6)  | 0.235 (4)  | 0.883 (4)  | 0.2 (2)          | 1    |
| O1   | 0.418 (10) | 0.455 (8)  | 0.874 (7)  | 0.5 (2)          | 1    |
| O2   | 0.577 (11) | 0.567 (9)  | 0.150 (7)  | 0.5 (2)          | 1    |
| O3   | 0.380 (12) | 0.484 (10) | 0.354 (8)  | 0.5 (2)          | 1    |
| O4   | 0.644 (14) | 0.533 (10) | 0.659 (8)  | 0.5 (2)          | 1    |
| O5   | 0.280 (11) | 0.801 (9)  | 0.567 (8)  | 0.5 (2)          | 1    |
| O6   | 0.741 (11) | 0.207 (9)  | 0.449 (8)  | 0.5 (2)          | 1    |
| O7   | 0.500 (11) | 0.224 (7)  | 0.174 (7)  | 0.5 (2)          | 1    |
| O8   | 0.485 (11) | 0.770 (7)  | 0.817 (8)  | 0.5 (2)          | 1    |
| O9   | 0.151 (11) | 0.250 (7)  | -0.001 (8) | 0.5 (2)          | 1    |
| O10  | 0.849 (10) | 0.736 (7)  | 0.997 (8)  | 0.5 (2)          | 1    |
| O11  | 0.184 (11) | 0.474 (7)  | 0.566 (7)  | 0.5 (2)          | 1    |
| O12  | 0.833 (11) | 0.514 (8)  | 0.414 (7)  | 0.5 (2)          | 1    |
| O13  | 0.004 (10) | 0.733 (9)  | 0.732 (7)  | 0.5 (2)          | 1    |
| O14  | 0.977 (10) | 0.299 (9)  | 0.255 (7)  | 0.5 (2)          | 1    |
| O15  | 0.333 (15) | 0.054 (9)  | 0.822 (9)  | 0.5 (2)          | 1    |
| O16  | 0.682 (15) | 0.960 (9)  | 0.183 (9)  | 0.5 (2)          | 1    |
| O17  | 0.357 (12) | 0.205 (8)  | 0.582 (8)  | 0.5 (2)          | 1    |
| O18  | 0.667 (13) | 0.794 (8)  | 0.407 (7)  | 0.5 (2)          | 1    |
| O19  | 0.194 (13) | 0.007 (11) | 0.227 (8)  | 0.5 (2)          | 1    |
| O20  | 0.812 (13) | 1.008 (11) | 0.769 (9)  | 0.5 (2)          | 1    |
| O21  | 0.267 (11) | 0.734 (8)  | 0.052 (7)  | 0.5 (2)          | 1    |
| O22  | 0.728 (12) | 0.275 (8)  | 0.976 (7)  | 0.5 (2)          | 1    |
| O23  | 0.060 (11) | 0.649 (7)  | 0.241 (8)  | 0.5 (2)          | 1    |
| O24  | 0.926 (11) | 0.345 (7)  | 0.746 (8)  | 0.5 (2)          | 1    |

quadrupole cleavage  $QS = 0.48 \text{ mm/s}$  (percentage occupancy of the crystal position  $A = 0.88\%$ ). There is also a signal with a significantly lower intensity related to iron cations, which are characterized by an oxygen environment in the form of trigonal bipyramids (percentage occupancy of this position is  $0.12\%$ ). These positions of iron cations have a smaller coordination number and, consequently, a smaller chemical shift ( $IS = 0.31 \text{ mm/s}$ ), as well as a

significant degree of distortion of the local environment ( $QS = 1.12 \text{ mm/s}$ ).

### 3.2. Results of the study of $\text{NaZnFe}_2(\text{VO}_4)_3$ using electron paramagnetic resonance method

The measurement data of samples of  $\text{NaZnFe}_2(\text{VO}_4)_3$  by electron paramagnetic resonance (EPR) in the temperature

**Table 3.** Basic bond lengths (Å) in the crystal structure of NaZnFe<sub>2</sub>(VO<sub>4</sub>)<sub>3</sub>

|                        |          |                       |          |
|------------------------|----------|-----------------------|----------|
| Na1–O6                 | 2.37 (5) | Zn4–O2                | 2.11 (6) |
| Na1–O17 <sup>i</sup>   | 2.36 (5) | Zn4–O8 <sup>vi</sup>  | 2.05 (7) |
| Na1–O18 <sup>ii</sup>  | 2.58 (5) | Zn4–O10 <sup>vi</sup> | 2.14 (5) |
| Na1–O20 <sup>ii</sup>  | 2.83 (7) | Zn4–O16               | 1.96 (7) |
| Na1–O24                | 2.67 (5) | Zn4–O21               | 1.96 (5) |
| Na2–O5                 | 2.45 (5) | Fe5–O4                | 2.01 (7) |
| Na2–O5                 | 2.45 (5) | Fe5–O4                | 2.01 (7) |
| Na2–O6 <sup>iii</sup>  | 2.24 (5) | Fe5–O8                | 2.11 (5) |
| Na2–O17 <sup>iii</sup> | 2.28 (5) | Fe5–O10               | 2.08 (7) |
| Na2–O18                | 2.26 (6) | Fe5–O13 <sup>i</sup>  | 1.79 (5) |
| Na2–O20                | 2.59 (8) | Fe5–O20               | 1.88 (6) |
| Fe1–O3                 | 2.06 (5) | Zn5–O4                | 2.01 (7) |
| Fe1–O5                 | 1.96 (7) | Zn5–O8                | 2.11 (5) |
| Fe1–O11                | 2.05 (6) | Zn5–O10               | 2.08 (7) |
| Fe1–O12 <sup>iv</sup>  | 2.04 (5) | Zn5–O13 <sup>i</sup>  | 1.79 (5) |
| Fe1–O14 <sup>iv</sup>  | 2.15 (6) | Zn5–O20               | 1.88 (6) |
| Fe1–O23                | 1.79 (6) | Fe6–O3                | 2.03 (7) |
| Zn1–O3                 | 2.06 (5) | Fe6–O7                | 1.89 (5) |
| Zn1–O5                 | 1.96 (7) | Fe6–O9                | 1.98 (7) |
| Zn1–O11                | 2.05 (6) | Fe6–O14 <sup>iv</sup> | 2.07 (4) |
| Zn1–O12 <sup>iv</sup>  | 2.04 (5) | Fe6–O19               | 1.90 (6) |
| Zn1–O14 <sup>iv</sup>  | 2.15 (6) | Zn6–O3                | 2.03 (7) |
| Zn1–O23                | 1.79 (6) | Zn6–O7                | 1.89 (5) |
| Fe2–O4                 | 1.97 (6) | Zn6–O9                | 1.98 (7) |
| Fe2–O6                 | 2.12 (6) | Zn6–O14 <sup>iv</sup> | 2.07 (4) |
| Fe2–O11 <sup>i</sup>   | 2.14 (5) | Zn6–O19               | 1.90 (6) |
| Fe2–O12                | 2.06 (7) | V1–O1                 | 2.00 (7) |
| Fe2–O13 <sup>i</sup>   | 2.03 (6) | V1–O4                 | 1.71 (6) |
| Fe2–O24                | 1.86 (6) | V1–O8                 | 2.68 (5) |
| Zn2–O4                 | 1.97 (6) | V1–O11                | 1.73 (6) |
| Zn2–O6                 | 2.12 (6) | V1–O17                | 1.66 (5) |
| Zn2–O11 <sup>i</sup>   | 2.14 (5) | V2–O2                 | 1.64 (7) |
| Zn2–O12                | 2.06 (7) | V2–O3                 | 1.77 (5) |
| Zn2–O13 <sup>i</sup>   | 2.03 (6) | V2–O12                | 1.92 (5) |
| Zn2–O24                | 1.86 (6) | V2–O18                | 1.46 (5) |
| Fe3–O1                 | 1.84 (5) | V3–O5                 | 1.50 (8) |
| Fe3–O2 <sup>v</sup>    | 2.11 (6) | V3–O8                 | 1.76 (5) |
| Fe3–O7 <sup>v</sup>    | 2.14 (6) | V3–O11                | 2.83 (5) |
| Fe3–O9 <sup>v</sup>    | 2.07 (5) | V3–O13                | 1.92 (4) |
| Fe3–O15                | 2.07 (7) | V3–O15 <sup>iii</sup> | 1.62 (6) |
| Fe3–O22                | 1.92 (6) | V4–O6                 | 1.82 (7) |
| Zn3–O1                 | 1.84 (5) | V4–O7                 | 1.74 (5) |
| Zn3–O2 <sup>v</sup>    | 2.11 (6) | V4–O12                | 2.57 (6) |
| Zn3–O7 <sup>v</sup>    | 2.14 (6) | V4–O14                | 1.74 (5) |
| Zn3–O9 <sup>v</sup>    | 2.07 (5) | V4–O16 <sup>ii</sup>  | 1.66 (6) |
| Zn3–O15                | 2.07 (7) | V5–O10 <sup>vii</sup> | 1.76 (6) |
| Zn3–O22                | 1.92 (6) | V5–O19 <sup>iii</sup> | 1.67 (7) |
| Fe4–O1 <sup>vi</sup>   | 2.14 (6) | V5–O21                | 1.63 (6) |
| Fe4–O2                 | 2.11 (6) | V5–O23                | 1.75 (5) |
| Fe4–O8 <sup>vi</sup>   | 2.05 (7) | V6–O9 <sup>viii</sup> | 1.67 (6) |
| Fe4–O10 <sup>vi</sup>  | 2.14 (5) | V6–O20 <sup>ii</sup>  | 1.75 (7) |
| Fe4–O16                | 1.96 (7) | V6–O22                | 1.77 (6) |
| Fe4–O21                | 1.96 (5) | V6–O24                | 1.82 (6) |
| Zn4–O1 <sup>vi</sup>   | 2.14 (6) |                       |          |

Note. Symmetry elements: (i)  $x + 1, y, z$ ; (ii)  $x, y - 1, z$ ; (iii)  $x, y + 1, z$ ; (iv)  $x - 1, y, z$ ; (v)  $x, y, z + 1$ ; (vi)  $x, y, z - 1$ ; (vii)  $x - 1, y, z - 1$ ; (viii)  $x + 1, y, z + 1$ .

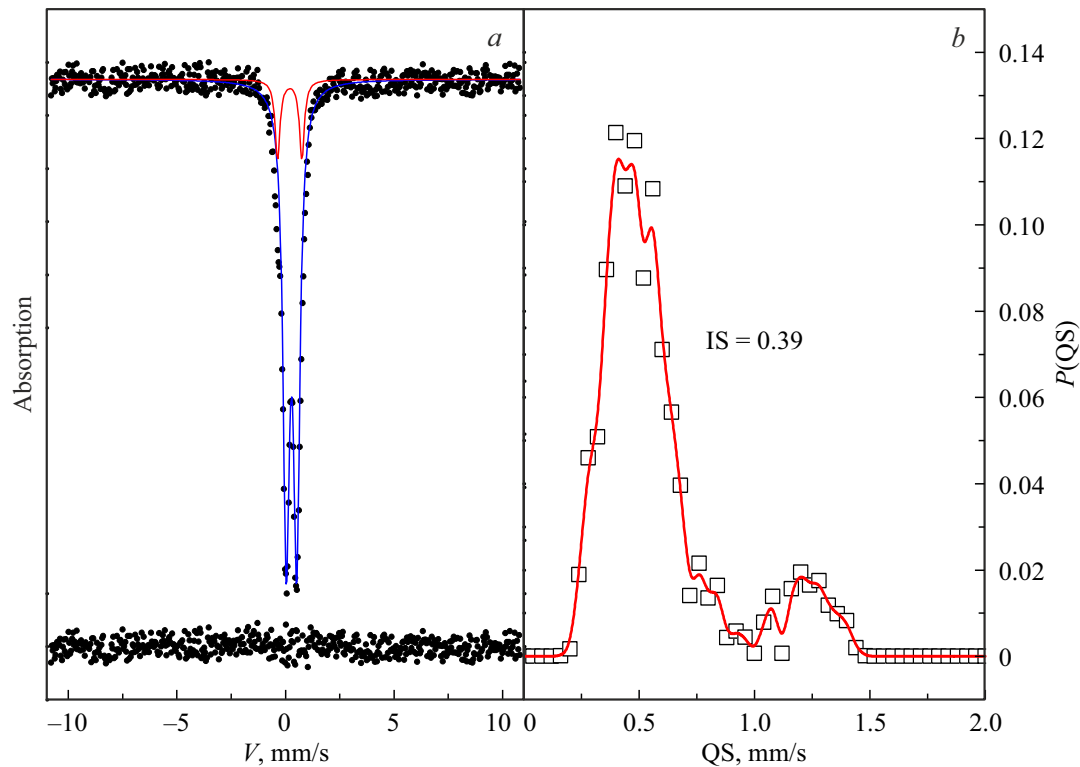


**Figure 3.** *a)* The Mössbauer spectrum of  $\text{NaZnFe}_2(\text{VO}_4)_3$  measured at room temperature. The colored lines show the components of the spectrum. The difference between the experimental and calculated spectrum is shown below. *b)* Probability distribution of quadrupole splits in the experimental spectrum.

**Table 4.** Mössbauer parameters of the compound  $\text{NaZnFe}_2(\text{VO}_4)_3$  at room temperature. (IS — isomeric chemical shift relative to  $\alpha\text{-Fe}$ .  $H$  — hyperfine field on the iron core. QS — quadrupolar splitting.  $W$  — absorption line width.  $A$  — percentage occupancy of non-equivalent positions)

| IS, mm/s<br>$\pm 0.01$ | $H$ , kOe<br>$\pm 5$ | QS, mm/s<br>$\pm 0.02$ | $W$ , mm/s<br>$\pm 0.02$ | $A$ , per.%<br>$\pm 0.05$ | Position            |
|------------------------|----------------------|------------------------|--------------------------|---------------------------|---------------------|
| 0.39                   | 0                    | 0.48                   | 0.35                     | 0.88                      | $\text{Fe}^{3+}(6)$ |
| 0.31                   | 0                    | 1.12                   | 0.28                     | 0.12                      | $\text{Fe}^{3+}(5)$ |

range 110–300 K are shown in Fig. 4. The observed EPR signal at room temperature in the  $X$ -range is a single Lorentz resonance line with a width of  $dH = 815$  Oe (the field distance between the extremes on the curve of the derivative of the absorption line) at  $T = 300$  K (Fig. 4, *a*).

The results of the study of temperature dependences of the main parameters of the first derivative of the EPR signal absorption  $d\chi''/dH$  — amplitude  $A$ , width  $dH$ , resonance field  $H_{\text{res}}$  in  $\text{NaZnFe}_2(\text{VO}_4)_3$  are shown in Fig. 4, *b–d*. The measurements showed that the amplitude  $A$  (the distance between the extremes along the ordinate axis on the curve line  $d\chi''/dH$ ) increases with decreasing temperature (Fig. 4, *b*); the resonant field corresponding to the intersection of the contour of the derivative  $d\chi''/dH$  with a zero line, in the temperature range 110–300 K does not change (Fig. 4, *c*); when the temperature decreases, the line width of the magnetic resonance signal  $dH$  monotonically

increases (Fig. 4, *d*). Such a shape of curves  $dH(T)$  was observed earlier in the compound  $\text{LiCuFe}_2(\text{VO}_4)_3$  [7]. The latter is probably due to the growth of local fields on the magnetic cations  $\text{Fe}^{3+}$  of the sample.

The use of the EPR method to study the compound  $\text{NaZnFe}_2(\text{VO}_4)_3$  allowed us to determine the value of the spectroscopic splitting factor Lande  $g = 1.991$  ( $T = 300$  K). The value of the factor  $g$ , close to 2, confirms that the observed resonance line corresponds to the signal from the ions  $\text{Fe}^{3+}$  ( $L = 0$ ).

### 3.3. Magnetic properties of $\text{NaZnFe}_2(\text{VO}_4)_3$ and behavior of temperature dependence of permittivity

In the compound  $\text{NaZnFe}_2(\text{VO}_4)_3$  vanadium cations  $\text{V}^{5+}$  are in the diamagnetic state (electronic configuration

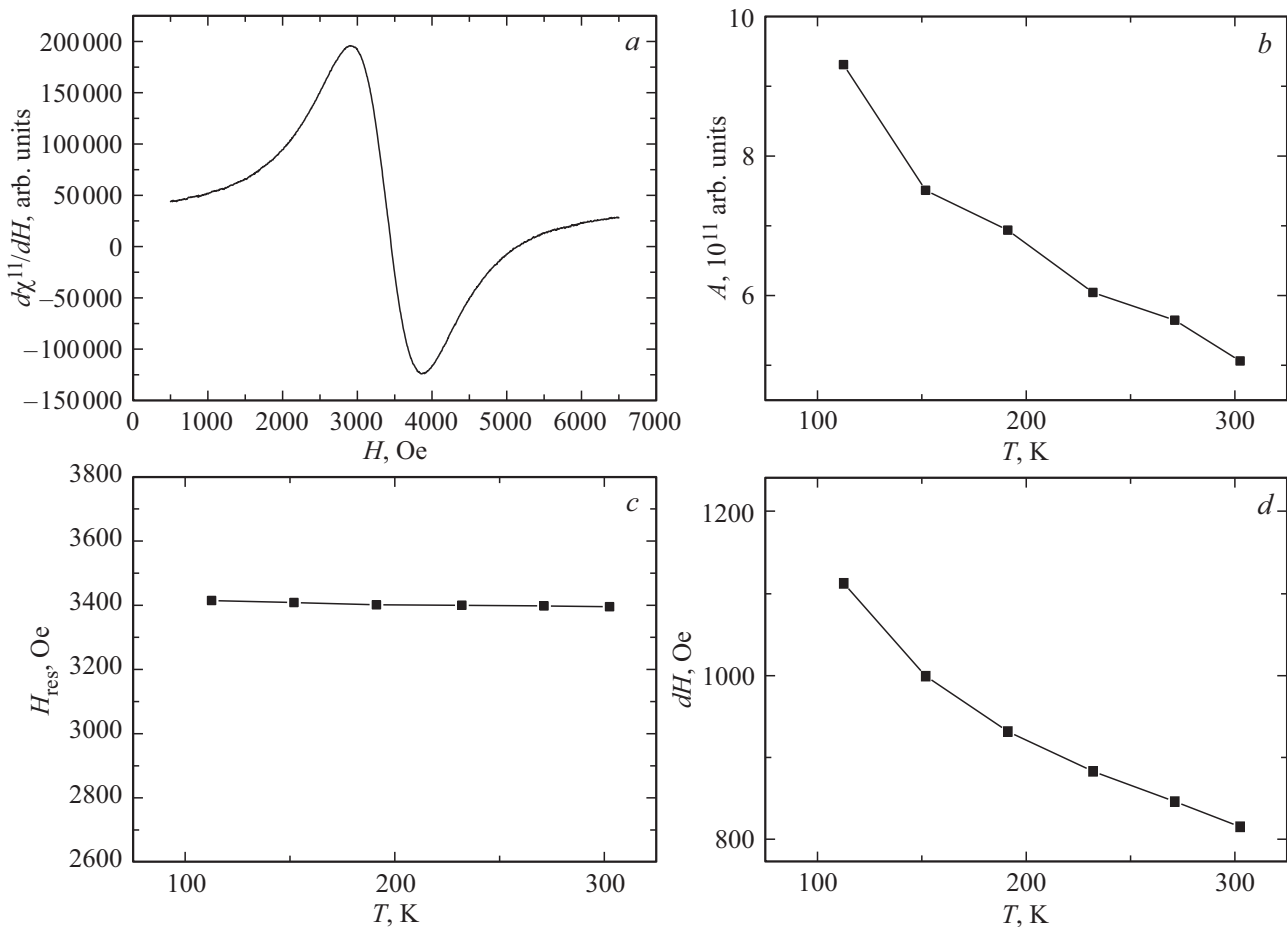


**Figure 4.** EPR spectrum in X-range at room temperature (a) and temperature dependences of amplitude  $A$  (b), resonance field  $H_{res}$  (c), line width  $dH$  (d) of the EPR signal in  $\text{NaZnFe}_2(\text{VO}_4)_3$ .

$3d^0$ ). The formation of magnetic properties involves iron cations  $\text{Fe}^{3+}$ , which are characterized by a high spin state  $S = 5/2$  (electronic configuration  $3d^5$ ), and occupy together with diamagnetic cations  $\text{Zn}^{2+}$  six unequal positions in the crystal lattice. The presence of zinc in the spin chains  $S = 5/2$  violates their uniformity, changes the distance between magnetic cations, weakening the magnetic interaction  $d^5 - d^5$ . Results of static magnetic measurements of  $\text{NaZnFe}_2(\text{VO}_4)_3$  are shown in Fig. 5.

Fig. 5, a shows the dependence of the magnetic moment  $M$  on the temperature  $T$ , measured in the magnetic field  $H = 500$  Oe when cooling a sample with a mass of  $m = 0.00738$  g in the absence of a magnetic field. Fig. 5, b shows the temperature course of the inverse magnetic susceptibility  $\chi^{-1}(T)$ , determined from static measurements of the magnetic moment of the sample as  $\chi^{-1}(T) = M(T)/Hm$ . According to the above measurement results the behavior of the curve  $\chi^{-1}(T)$  in the temperature range  $T > 30$  K can be described by Curie–Weiss law. The asymptotic temperature of the Neel, defined as the intersection point of the axis  $T$  with the asymptote to the curve  $\chi^{-1}(T)$  in the high temperature region, has a negative value  $\theta = -89$  K and indicates the predominant role of

antiferromagnetic exchange interactions in the magnetic system  $\text{NaZnFe}_2(\text{VO}_4)_3$ . Curie–Weiss constant  $C = 0.0159$  K corresponds to the value of the effective magnetic moment (molar value)  $\mu_{\text{eff}(\text{exp})} = 8.363 \mu_B$ . The calculated value of the effective magnetic moment of the formula unit of the compound  $\text{NaZnFe}_2(\text{VO}_4)_3$   $\mu_{\text{eff}(\text{cal.})} = 8.358 \mu_B$  using the known value of the effective magnetic moment of the ions  $\text{Fe}^{3+}$   $\mu_{\text{eff}(\text{cal.})}^{\text{Fe}^{3+}} = 5.91 \mu_B$  (spectroscopic splitting factor  $g = 2$ ) [13]. The calculated and experimental values of the effective magnetic moment match quite well according to the evaluation, confirming the main role of trivalent iron cations  $\text{Fe}^{3+}$  in the formation of paramagnetic properties of the sample under study.

It was also experimentally found that a nonlinear dependence of the magnetic moment on temperature (Fig. 5) and the impact of the thermal background of the sample (cooling of the sample without a magnetic field — ZFC and in the presence of a magnetic field — FC) is observed in the low temperature region ( $T < 30$  K) (Fig. 5, c). The magnetic moment measured in the magnetic field  $H = 10$  Oe (the mass of the sample  $m = 0.090$  g), under the condition of ZFC, increases with decreasing temperature, reaching a maximum at temperature  $T = 5.7$  K, then decreases.

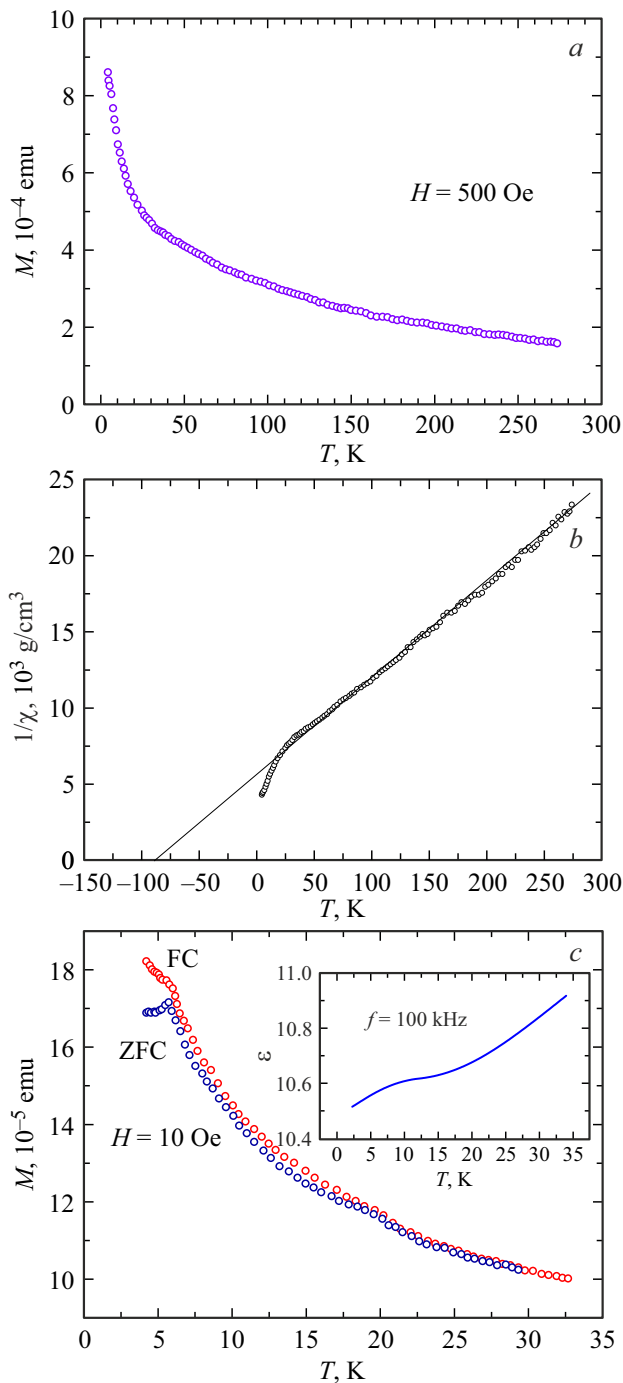


**Figure 5.** Temperature dependences of the magnetic moment  $M$  (a,c) measured in the magnetic field  $H = 500$  Oe (a) and  $H = 10$  Oe (c), and reverse magnetic susceptibility  $\chi^{-1}$  (b) in  $\text{NaZnFe}_2(\text{VO}_4)_3$ . The dependence of the magnetic moment on the cooling conditions of the sample (c) (ZFC — cooling without a field and FC — cooling in an external magnetic field) is shown. In the insert (c): the temperature dependence of the dielectric constant  $\epsilon$ , measured at  $f = 100$  kHz.

The divergence of the curves  $M(T)$  under ZFC and FC conditions takes place at the critical temperature — freezing temperature  $T_F \approx 6$  K (Fig. 5,c). The character of

temperature dependences of the magnetic moment  $M(T)$  in  $\text{NaZnFe}_2(\text{VO}_4)_3$  is typical for magnetic states of the spin glass type [1–3]. Evaluation of the frustration level of magnetic interactions  $f$  between pairs  $d^5-d^5$  using the ratio  $f = |\theta|/T_F$  [14,15] shows a significant value —  $f \approx 15$ .

The inset of Fig. 5, c shows the temperature dependence of the dielectric constant  $\epsilon$  measured in the temperature range  $2.3 \text{ K} < T < 33 \text{ K}$  at a frequency of  $f = 100$  kHz in a polycrystal  $\text{NaZnFe}_2(\text{VO}_4)_3$ . When the temperature decreases, a decrease of the dielectric constant is observed, while there is no anomaly at the critical temperature  $T_F \approx 6$  K, which confirms the absence of a transition of the magnetic subsystem to a state with a long-range magnetic order. The behavior of the dependence curve —  $\epsilon(T)$  is characteristic of the magnetic transition to the spin-glass state. Absence of long-range magnetic order in the compound  $\text{NaZnFe}_2(\text{VO}_4)_3$  is probably related to the non-statistical distribution of high-spin  $\text{Fe}^{3+}$  and diamagnetic ions  $\text{Zn}^{2+}$  across six nonequivalent crystallographic positions, leading to magnetic heterogeneity, competition and a high level of frustration of exchange magnetic interactions that contribute to the formation of disordered magnetism.

## 4. Conclusion

The compound  $\text{NaZnFe}_2(\text{VO}_4)_3$ , synthesized by reaction in the solid phase, crystallizes at room temperature in a triclinic syngony with a spatial symmetry group  $P1$ .

Features of the crystal structure of  $\text{NaZnFe}_2(\text{VO}_4)_3$ , the presence of magnetic ions  $\text{Fe}^{3+}$ , located in six nonequivalent crystallographic positions mixed together with diamagnetic ions  $\text{Zn}^{2+}$ , lead to the realization of both an inhomogeneous magnetic state and a state of local violation of charge neutrality.

In the temperature range of  $T > 30$  K magnetic subsystem  $\text{NaZnFe}_2(\text{VO}_4)_3$  formed by chains of iron cations  $\text{Fe}^{3+}$  with an effective magnetic moment (molar value)  $\mu_{\text{eff}(\text{exp})} = 8.363 \mu_B$ , bound by the predominant antiferromagnetic interaction, is in a paramagnetic state described by Curie–Weiss law. A transition from the paramagnetic state to the magnetic spin-glass state is observed when the temperature decreases.

## Funding

The work was conducted within the framework of the scientific theme of the state assignment of the Kirensky Institute of Physics of SB RAS.

The authors thank the Krasnoyarsk Regional Research Equipment Sharing Center of the Federal Research Center Krasnoyarsk Science Center of the Siberian Branch of the Russian Academy of Sciences for the provided equipment for measurements.

## Conflict of interest

The authors declare that they have no conflict of interest.

## References

- [1] I.Ya. Korenblit, E.F. Shender. UFN **157**, 267 (1989). (in Russian).
- [2] V.S. Dotsenko. UFN **163**, 1 (1993). (in Russian).
- [3] J.A. Mydosh. Spin-Glasses: An Experimental Introduction, Taylor and Francis. N.Y. (1993). 256 p.
- [4] A. Arauzo, J. Bartolomé, J. Luzón, T. Drokina, G.A. Petrakovskii, M.S. Molokeev. JMMM **515**, 167273 (2020).
- [5] A. Norlund Christensent, T. Johansson, B. Lebech. J. Phys. C **9**, 2601 (1976).
- [6] G. Petrakovsky, L. Bezmaternykh, I. Gudim, O. Bayukov, A. Vorotynov, A. Bovina, R. Shimchak, M. Baran, K. Ritter. FTT **48**, 1795 (2006). (in Russian).
- [7] T.V. Drokina, G.A. Petrakovsky, O.A. Bayukov, A.M. Vorotynov, D.A. Velikanov, M.S. Molokeev, FTT **58**, 1913 (2016). (in Russian).
- [8] A. Koshelev, L. Shvanskaya, O. Volkova, K. Zakharov, F. Theuss, C. Koo, R. Klingeller, S. Kamusella, H.-H. Klauss, S. Kundu, S. Bachhar, A.V. Mahajan, P. Khuntia, D. Khanam, B. Rahaman, T. Saha-Dasgupta, A.N. Vasiliev. J. Alloys Comp. **842**, 155763 (2020).
- [9] T.V. Drokina, D.A. Velikanov, O.A. Bayukov, M.S. Molokeev, G.A. Petrakovsky, FTT, **63**, 754 (2021). (in Russian).
- [10] D.A. Velikanov. Inorg. Mater. Appl. Res. **11**, 801 (2020).
- [11] F.D. Martin, H. Müller-Buschbaum. Z. Naturforschung B **50**, I, 51 (1995).
- [12] Bruker AXS TOPAS V4: General profile and structure analysis software for powder diffraction data. — User's Manual. Bruker AXS, Karlsruhe, Germany. (2008).
- [13] K.P. Belov, M.A. Belyanchikova, R.Z. Levitin, S.A. Nikitin. Redkozemel'nye ferromagnetiki i antiferromagnetiki. Nauka, M., (1965). 420 p. (in Russian).
- [14] J.E. Greedan, A.P. Ramirez. Comm. Condens. Mater. Phys. **18**, I, 21 (1996).
- [15] J.E. Greedan. J. Mater. Chem. **11**, 37 (2000).

*Translated by A.Akhtyamov*